Arch Appl Mech (2013) 83:1415–1438
DOI 10.1007/s00419-013-0755-4

ORIGINAL

Francesco Portioli · Claudia Casapulla · Lucrezia Cascini · Mario D'Aniello · Raffaele Landolfo

Limit analysis by linear programming of 3D masonry structures with associative friction laws and torsion interaction effects

Received: 21 November 2012 / Accepted: 8 May 2013 / Published online: 23 May 2013

Abstract In this paper, a formulation for limit analysis of three-dimensional masonry structures discretized as rigid block assemblages interacting through no-tension and frictional contact interfaces is developed. Linear and piecewise linearized yield functions are used for rocking, sliding and torsion failure. A simple yield condition has been defined to take into account interaction effects of shear force with torsion and bending moment. Associative flow rules are considered for strain rates. On the basis of the developed governing equations, the limit analysis problem has been formulated as a nonlinear mathematical program. An iterative solution procedure based on linear programming is used to solve the limit analysis problem and to take into account nonlinearities due to the influence of bending moments and shear stresses on torsion strength. The results of experimental investigations on out-of-plane masonry walls constrained at one edge and different examples from literature were considered for validation. Comparison with existing formulations is carried out.

Keywords Three-dimensional rigid block assemblages · Dry-jointed masonry structures · Limit analysis · Associative flow rules · Interaction effects · Linear programming · Iterative solution procedure

1 Introduction

Limit analysis of rigid block assemblages with tensionless and frictional contact interfaces is an accurate and robust computational approach for the prediction of collapse load and failure mechanism of masonry structures. This approach has been extensively used to analyze the behavior of two-dimensional (2D) masonry structures, especially in the case of historic constructions with dry or weak mortar joints [1–4].

Although different formulations can be found in the literature for three-dimensional (3D) rigid block assemblages as well, the extension and the practical application of computational limit analysis to large-scale masonry structures still represent a challenging and open issue.

As a matter of fact, the formulation of the limit analysis problem in terms of mathematical programming with respect to three-dimensional rigid block assemblages involves several issues: among those, the modelling of contact interfaces, the definition of yield functions and interaction effects, and the flow rule assumptions for plastic strains. Depending on the selected modelling approaches, the limit analysis problem may lead to a linear or nonlinear mathematical program, with unique or multiple solutions. The number and sources of nonlinearity in the governing equations for yield conditions are strictly related to the model adopted for contact interface interactions.

F. Portioli (✉) · C. Casapulla · L. Cascini · M. D'Aniello · R. Landolfo
Department of Structures for Engineering and Architecture
University of Naples "Federico II", Via F. Vecchio 36, 80134 Naples, Italy
Tel.: +39.081.25.38.916
Fax: +39.081.25.38.989
E-mail: fportiol@unina.it

Different formulations have been proposed, on the basis of the number of contact points and stress components at interfaces [5–7]. Among those, the convex contact formulation is of particular interest for the present study. In such a case, a single point located at the center of each interface is used to model interactions among rigid blocks. The stress resultant vector is characterized by six components, including normal and shear forces as well as bending and torsion moments, corresponding in a virtual work sense to the internal degrees of freedom of the contact interface. The behavior at interfaces is governed by yield functions of contact static variables and by flow rules, which define the relationship between resultant strain rates and plastic flow multipliers in limit analysis.

The adoption of a convex contact interface model generally involves the definition of bending, shear and torsion failure conditions expressed as a function of static variables. Besides, a further important issue is the evaluation of interaction effects, such as those among torsion, shear and bending moments, which can be taken into account using a proper formulation of failure surfaces. The modelling of interaction effects, which is focused in the present study, represents a key aspect in the formulation of limit analysis problems, since it may involve strong nonlinearities in governing equations.

Another important aspect in computational limit analysis by rigid block assemblages is the modelling of flow rules. Both associative and non-associative behavior can be formulated in relation to the assumptions made on the resultant strain rates corresponding to different failure mechanisms. These assumptions involve important implications on the value of collapse load multiplier. In general, the collapse load factor from the associative model represents an upper bound for the non-associative model [6,8].

On the basis of the governing conditions mentioned above and depending on the type of considered relationship between variables and yield functions, the limit analysis problem can be formulated in terms of a mixed complementarity problem (MCP) with linear or nonlinear constraints [9].

In case of associative friction laws and linear constraints, the MCP is symmetric and can be uncoupled into two dual linear programming problems, corresponding to the formulation of the upper and lower bound theorems of limit analysis, whose unique solution is the optimal load multiplier [5].

If the interaction at interfaces is characterized by non-associative flow rules, the problem of computing the collapse loads of discrete rigid block systems turns into a non-symmetric MCP. In this case, the solution to the limit analysis problem is not unique, and the problem of calculating the minimum collapse load corresponding to the different solutions arises.

Different formulations and solution methods for the MCP have been developed in the literature specifically devoted to three-dimensional rigid block assemblages. Among those [10,11], it is worth to mention for the present study the formulation developed by Orduña and Lourenço [7,12], which is based on no-tension frictional convex interfaces. The authors proposed a torsion failure yield condition and developed linearized yield surfaces to consider torsion-shear and torsion-bending moment interactions. The model takes into account non-associated flow rules and limited compressive stresses at interfaces. A load path procedure is developed based on the solution of different MCPs with increasing variable loads, thus following the loading history on the structure. A number of validation examples are showed, and a good agreement with FEM models used for comparison is obtained.

Although the above formulations, which takes into account nonlinearity associated with yielding constraints as well as interaction effects and non-associative flow rules, provide a good prediction of collapse load multipliers and failure modes for masonry structures, the solution of the associated MCPs by nonlinear programming generally involves too long CPU time through standard solution routines when applied to rigid block assemblages with a large number of elements [12]. As a consequence, the application of limit analysis to large-scale problems is mainly limited to 2D assemblages [13], and only few applications on 3D rigid block structures can be found in the literature [5,7,10–12].

In addition, it should be noted that the most part of three-dimensional limit analysis formulations have been validated against experimental tests which essentially refer to in-plane loaded structures, also due to the lack of available data at the time of application. Considering that new experimental investigations have been recently carried out on dry-jointed masonry panels which also take into account out-of-plane failures [14,15], it would be interesting to compare the existing testing outcomes with the results predicted by numerical models in the field.

All these considered, the main aim of the present study is to develop a simplified formulation for the limit analysis of three-dimensional rigid block assemblages and to evaluate the accuracy of the proposed modelling approach in predicting the response of masonry wall panels out-of-plane loaded. The study comes within a research activity focused on the use of iterative and sequential linear programming for limit analysis of masonry structures [16].

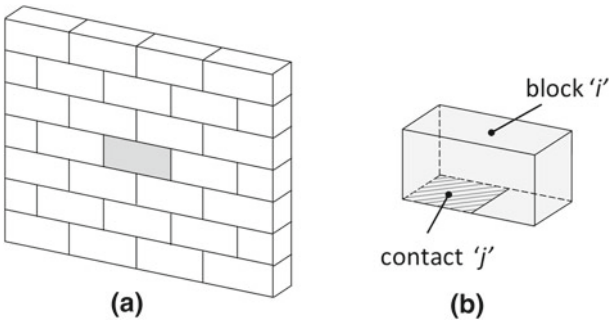

Fig. 1 **a** Three-dimensional rigid block assemblage. **b** Block and contact interfaces

To overcome difficulties related to the solution of MCPs in three-dimensional analysis, a simplified formulation for limit analysis of spatial rigid block assemblages based on convex contact interfaces and linear programming is presented.

The key aspects of the proposed formulation are as follows. Linearized yield conditions for torsion, torsion-shear and torsion-bending moment interactions have been developed on the basis of the work by Casapulla [17] and Casapulla and D'Ayala [18] and herein extended to 3D computational limit analysis. Associative flow rules are used to reduce the problem to a skew symmetric mathematical program. Moreover, a novel iterative computational procedure based on the solution of linear programs is proposed to take into account nonlinearities due to interaction effects of torsion strength with shear forces and bending moments. A computer program has been developed on the basis of the proposed formulation which provides as output failure modes and collapse load multipliers.

The paper is organized as follows. The implemented modelling approach and the limit analysis formulation are presented in Sects. 2 and 3. The adopted solution procedure is illustrated in Sect. 4.

Finally, in Sect. 5, the results of the numerical analysis on different case studies taken from the literature and relevant to wall panels out-of-plane loaded are presented to evaluate the accuracy and efficiency of the developed formulation. Moreover, the results of an experimental investigation carried out on dry-jointed tuff masonry walls constrained at one edge are presented for validation.

2 The rigid block limit analysis model

The structural model consists of an assemblage of rigid blocks i connected by convex contact interfaces j (Fig. 1). Failure is concentrated at block interfaces and includes different types of collapse modes, namely joint separation, rocking, sliding and twisting, and combinations of them. No-tension behavior and infinite compressive strength are assumed for contacts.

The details of the modelling approach adopted for the formulation of the limit analysis problem in terms of linear programming are presented in the following.

The formulation of governing equations is based on the work by Ferris & Tin-Loi [9], and it has been extended to three-dimensional block assemblages.

The problem is formulated in terms of equilibrium equations between external and internal forces and by means of the kinematic equations which express the compatibility relationship of contact strain rates and block degrees of freedom.

To model the behavior at interfaces, yield functions of contact static variables are defined and flow rules are provided, governing the increment of plastic strain when yielding occurs. Although the formulation can be developed for arbitrarily shaped interfaces, the particular case of rectangular contacts is tackled in this paper.

Static and kinematic variables as well as equilibrium equations, constitutive laws and flow rules are given in matrix form, according to the expressions reported in the following.

2.1 Static and kinematic variables

The static variables are represented by the internal forces acting at interface j and referred to the center of contact (Fig. 2a). These variables are the shear force V_j, the normal force N_j, the bending moment M_j and the torsion moment M_{Tj}. Those are all collected in the vector $\mathbf{x}_j$.

$$\mathbf{x_j} = \left[V_{1j} \;\; V_{2j} \;\; N_j \;\; M_{1j} \;\; M_{2j} \;\; M_{\mathrm{Tj}} \right]^T \tag{1}$$

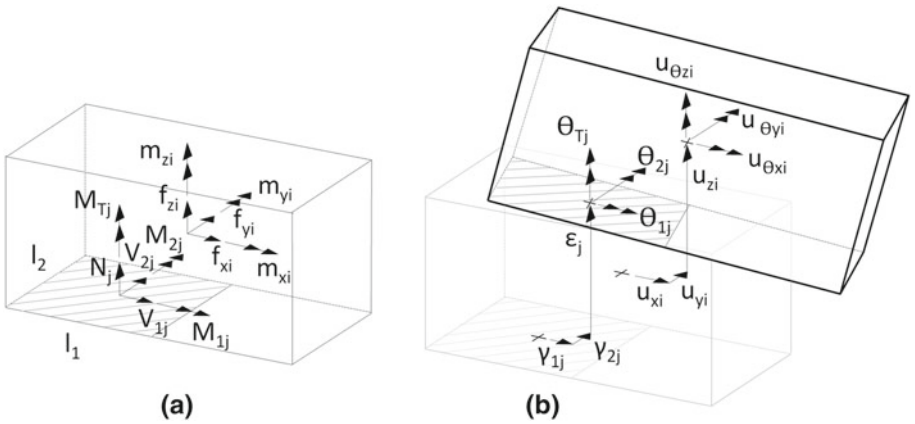

Fig. 2 Static and kinematic variables at block i and contact interface j

The corresponding kinematic variables in a virtual work sense are the relative displacement rates at interfaces, namely the relative tangential, normal and angular rates γ_j, ε_j and θ_j (Fig. 2b), which are collected in the vector $\mathbf{q}_j$:

$$\mathbf{q_j} = \left[\gamma_{1j}\ \gamma_{2j}\ \varepsilon_j\ \theta_{1j}\ \theta_{2j}\ \theta_{\mathrm{Tj}}\right]^T \tag{2}$$

The loads are applied to the centroid of the rigid block i and are indicated with the vector $\mathbf{f_i}$:

$$\mathbf{f_i} = \left[f_{\mathrm{xi}}\ f_{\mathrm{yi}}\ f_{\mathrm{zi}}\ m_{\mathrm{xi}}\ m_{\mathrm{yi}}\ m_{\mathrm{zi}}\right]^T \tag{3}$$

The loads $\mathbf{f_i}$ are expressed as the sum of the known dead loads $\mathbf{f_{Di}}$ and live loads $\mathbf{f_{Li}}$ amplified by an unknown scalar multiplier α.

$$\mathbf{f_i} = \mathbf{f_{Di}} + \alpha\mathbf{f_{Li}} \tag{4}$$

The displacement rates at the centroid of the block i, that are work conjugated to the nodal loads $\mathbf{f_i}$, are collected in the vector $\mathbf{u_i}$:

$$\mathbf{u_i} = \left[u_{\mathrm{xi}}\ u_{\mathrm{yi}}\ u_{\mathrm{zi}}\ u_{\theta\mathrm{xi}}\ u_{\theta\mathrm{yi}}\ u_{\theta\mathrm{zi}}\right]^T \tag{5}$$

2.2 Equilibrium equations

For a block i and a contact j, the equilibrium equations of internal and external forces can be expressed in the matrix form:

$$\mathbf{A_{i/j}x_j} = \mathbf{f_i} \tag{6}$$

where $\mathbf{A_{i/j}}$ is a (6×6) equilibrium matrix with coefficients determined by the geometry of the blocks [5].

For the whole structure, the equilibrium in the matrix form gives:

$$\mathbf{A}_{6b\times 6c}\mathbf{x}_{6c} = \mathbf{f}_{6b} \tag{7}$$

being b the number of blocks and c the number of contacts, and it is obtained through assembly of matrices for each block.

2.3 Yield conditions

Under the assumption of Coulomb frictional and tensionless contact interface behavior, several possible failure conditions may govern the collapse mechanisms between each couple of blocks. In case of a 3D model, the potential failure conditions may involve the pure shear failure with relative displacements (in-plane and out-of-plane) tangential to the interfaces, the pure bending moment failure (in-plane and out-of-plane and Heyman's type) and the pure torsion failure about the centroid of the interfaces. Of course, a combinations of these modes is also likely to occur.

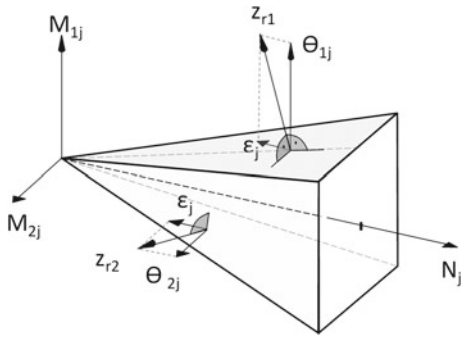

Fig. 3 Yield surfaces for pure bending moments with associated displacement rates

In the present formulation, the behavior at contact interfaces is governed by yield functions which take into account joint separation, sliding, rocking and torsion failure modes and combinations of them. A special focus is devoted to the problem of interaction and, in particular, to the interaction of the torsion strength with the shear forces and bending moments. A novel formulation, in case of associative frictional sliding only, is proposed and described in the following.

In matrix notation, the limit conditions at contact interface j can be written as:

$$\mathbf{y}_j = \mathbf{N}_j^T \cdot \mathbf{x}_j \leq \mathbf{0} \tag{8}$$

being $\mathbf{N}_j^T$ the yield function matrix.

The extension of Eq. (8) to the whole structure is straightforward. Coefficients of yield function matrix are specified in the following sections for the different failure conditions.

2.3.1 Pure bending moment

The bending moment on interface j is described by its components M_{1j} and M_{2j} along the reference axes x_1 and x_2, respectively (Fig. 2a).

The pure bending moments yield functions express the condition that components of bending moment on the contact cannot be greater than the corresponding resistant moments. Under the assumption of infinite compressive strength, resistant moments can be obtained as the product of normal force and the half length of the contact interface [6].

In particular, the following yield functions have been considered for bending moment condition:

$$\begin{aligned} y_j^{r,1,2} &= -\frac{l_2}{2} \cdot N_j \pm M_{1j} \leq 0 \\ y_j^{r,3,4} &= -\frac{l_1}{2} \cdot N_j \pm M_{2j} \leq 0 \end{aligned} \tag{9}$$

The set of proposed yield functions is represented in Fig. 3.

2.3.2 Pure shear

The shear force on interface j is described by its components V_{1j} and V_{2j} along the reference axes x_1 and x_2, respectively (Fig. 2a).

Under the hypothesis of isotropic friction and cohesionless behavior, the interface failure is governed by the Coulomb's law which can be represented by a cone yield function in the three-dimensional space of normal force N_j and shear components V_{1j} and V_{2j}.

This yield function can be expressed in the form:

$$y_j^s = \sqrt{V_{1j}^2 + V_{2j}^2} - \mu_j N_j \leq 0 \tag{10}$$

where $\mu_j = \tan \phi_j$ is the friction coefficient on interface j.

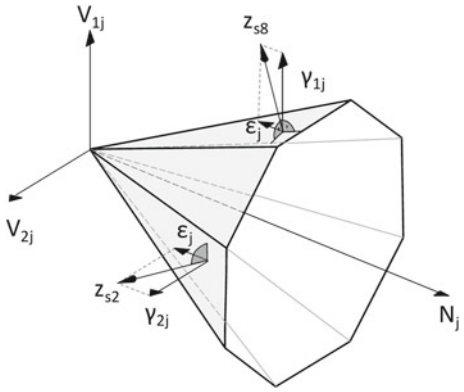

Fig. 4 Yield surfaces for pure shear with associated strain rates

To reduce the problem to a linear program, the yield function given by Eq. (10) has been linearized with 8 hyperplanes [5,7] obtained through the following relationships (Fig. 4):

$$y_j^{s,k} = \cos\frac{k\pi}{4}\cdot V_{1j} + \sin\frac{k\pi}{4}\cdot V_{2j} - \mu_j N_j \le 0 \qquad k = 1, 2, \ldots, 8 \tag{11}$$

where k is hyperplane number.

2.3.3 Pure plastic torsion

For the yield domains related to pure plastic torsion, torsion-shear and torsion-bending moment interactions, the assumptions presented in Casapulla [17] and Casapulla and D'Ayala [18] are herein revised and extended to 3D computational limit analysis.

Both shear force and torsion moment strengths of an interface are provided by shear stresses. When the contact interface j is only subjected to a compressive force N_j and to a torsion moment M_{Tj}, the centroid of the interface is coincident with the center of plastic torsion, and the corresponding shear stress components τ_{1j} and τ_{2j} are still governed by the Coulomb's law (Eq. 10), i.e.,

$$\sqrt{\tau_{1j}^2 + \tau_{2j}^2} - \sigma_j \mu_j \le 0 \tag{12}$$

where σ_j is the normal stress derived by a uniform distribution of the normal force N_j.

The direction of the shear stress vectors at each point is perpendicular to their distance from the center of torsion and parallel to the relative tangential flows, according to Coulomb's law. Thus, with reference to the point $P(x_1, x_2)$ in Fig. 5, the torsion moment strength can be expressed by the relation:

$$\begin{aligned} M_{\mathrm{T0j}} &= 4\tau_{0j}\int_0^{l_1/2}\mathrm{d}x_1\int_0^{l_2/2}\sqrt{x_1^2+x_2^2}\,\mathrm{d}x_2 \\ &= \frac{\tau_{0j}}{2}\int_0^{l_1/2}\left[l_2\sqrt{4x_1^2+l_2^2} + 4x_1^2\ln\frac{l_2+\sqrt{4x_1^2+l_2^2}}{2x_1}\right]\mathrm{d}x_1 \\ &= \frac{\tau_{0j}}{12}\left[l_1^3\ln\frac{l_2+\sqrt{l_1^2+l_2^2}}{l_1} + l_2^3\ln\frac{l_1+\sqrt{l_1^2+l_2^2}}{l_2} + 2l_1l_2\sqrt{l_1^2+l_2^2}\right] \end{aligned} \tag{13}$$

where $\tau_{0j} = \mu_j \cdot \sigma_j$ is the limit shear stress
Eq. (13) can be rewritten as:

$$M_{\mathrm{T0j}} = V_{0j} c_{\mathrm{Tj}} \tag{14}$$

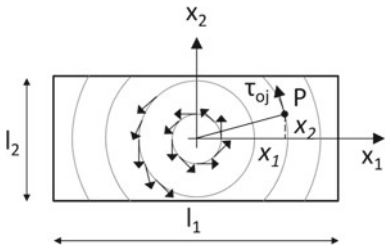

Fig. 5 Shear stresses on a *rectangular* contact interface subject to axial compression and pure torsion moment

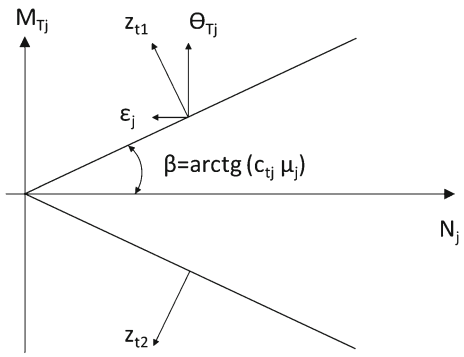

Fig. 6 Yield surface for pure torsion with associated strain rates

where V_{0j} and c_{Tj} are the pure shear strength and the arm of the internal couple, respectively, given by:

$$V_{0j} = \mu_j N_j \tag{15}$$

$$c_{\mathrm{Tj}} = \frac{1}{12 l_1 l_2}\left[l_1^3 \ln \frac{l_2 + \sqrt{l_1^2 + l_2^2}}{l_1} + l_2^3 \ln \frac{l_1 + \sqrt{l_1^2 + l_2^2}}{l_2} + 2 l_1 l_2 \sqrt{l_1^2 + l_2^2} \right] \tag{16}$$

Hence, the yield function assumed for torsion moment is given by the expression:

$$y_j^{t,1,2} = -c_{\mathrm{Tj}} \cdot \mu_j \cdot N_j \mp M_{\mathrm{Tj}} \leq 0 \tag{17}$$

and represented by the surface in Fig. 6.

2.3.4 Torsion-shear-bending moment interaction

In the following, the yield functions which take into account interaction effects between torsion moment and shear force as well as torsion and bending moment are formulated according to the approaches available in the literature. Afterward, combining the previous formulations, a novel yield function which considers as a whole the interactions among torsion-shear-bending moment is proposed.

2.3.4.1. Torsion-shear interaction When the contact interface j is subjected to torsion moment and shear force, the center of plastic torsion is away from the center of the interface, as shown in Fig. 7 (point C_t), but the shear stress vectors at each point are still orthogonal to their distance from this center. Thus, the two components of shear force resultant along the axes x_1 and x_2 are given by the equilibrium conditions:

$$V_{1j} = \tau_0 \int_{y_{1,c}}^{y_{1,c}+l_1} \mathrm{d}y_1 \int_{y_{2,c}}^{y_{2,c}+l_2} \frac{y_2}{\sqrt{y_1^2 + y_2^2}} \mathrm{d}y_2 = \tau_0 \int_{y_{1,c}}^{y_{1,c}+l_1} \left[\sqrt{y_1^2 + \left(y_{2,c} + l_2\right)^2} - \sqrt{y_1^2 + y_{2,c}^2} \right] \mathrm{d}y_1 \tag{18}$$

$$V_{2j} = \tau_0 \int_{y_{2,c}}^{y_{2,c}+l_2} \mathrm{d}y_2 \int_{x_c}^{x_c+a} \frac{y_1}{\sqrt{y_1^2 + y_2^2}} \mathrm{d}y_1 = \tau_0 \int_{y_{2,c}}^{y_{2,c}+l_2} \left[\sqrt{\left(y_{1,c} + l_1\right)^2 + y_2^2} - \sqrt{y_{1,c}^2 + y_2^2} \right] \mathrm{d}y_2 \tag{19}$$

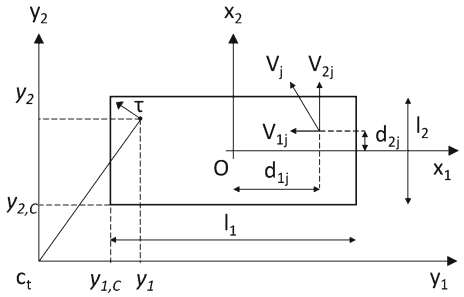

Fig. 7 Shear stress resultants on a *rectangular* contact interface subject to axial compression, shear and torsion

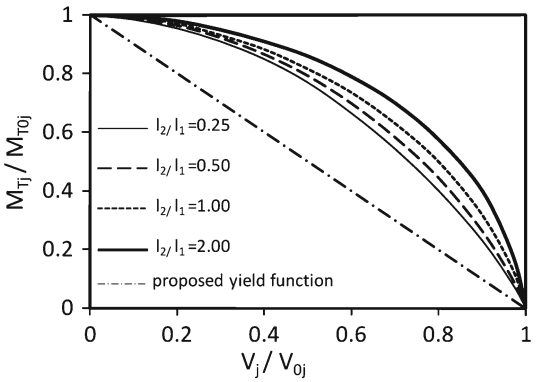

Fig. 8 Non-dimensional torsion-shear interaction *curves* for different interface aspect ratios [17]

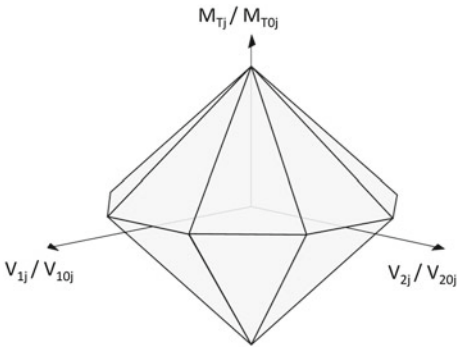

Fig. 9 Linearized yield surface for torsion and shear interaction

while the equilibrium equation about the torsion center C can be written as:

$$M_{\mathrm{Tj}} + V_{1j}\left(y_{2,c} + \frac{l_2}{2}\right) + V_{2j}\left(y_{1,c} + \frac{l_1}{2}\right) = \tau_0 \int_{y_{2,c}}^{y_{2,c}+l_2} \mathrm{d}y_2 \int_{y_{1,c}}^{y_{1,c}+l_1} \sqrt{y_1^2 + y_2^2}\,\mathrm{d}y_1 \tag{20}$$

where

$$M_{\mathrm{Tj}} = V_{1j} d_{2j} + V_{2j} d_{1j} \tag{21}$$

For further details related to the development of Eqs. (18), (19) and (20), a comprehensive discussion is reported in Casapulla [17], where a bijective mapping between the application point of the eccentric shear force and the torsion center was numerically defined for a given interface aspect ratio, and it will not be reviewed here.

Also, a family of interaction curves was numerically obtained for different interface aspect ratios represented in non-dimensional form in Fig. 8. These curves could be expressed by the following formulation:

$$M_{\mathrm{Tj}}/M_{\mathrm{T0j}} = 1 + a_1\left(V_j/V_{0j}\right) + a_2\left(V_j/V_{0j}\right)^2 + \cdots .. = 1 + \sum_{k=1}^{n} a_k\left(V_j/V_{0j}\right)^k \tag{22}$$

To reduce the limit analysis problem to a linear program, also in this case, a linearization of Eq. (22) is necessary. Different discretization approaches can be adopted, as the three linear piecewise function proposed by Orduña and Lourenço [7].

In this study, the straight line in Fig. 8 has been assumed as representative of the torsion-shear yield domain. Although this yield function does not take into account the interface aspect ratio, it provides a simpler formulation of the mathematical problem because it reduces the number of governing conditions being, at the same time, on the safe side.

Thus, the yield function for torsion-shear interaction can be expressed in the form:

$$y_j^{\mathrm{ts}} = \pm M_{\mathrm{Tj}} - M_{\mathrm{T0j}}\left(1 - \frac{\sqrt{V_{1j}^2 + V_{2j}^2}}{V_{0j}}\right) \leq 0 \tag{23}$$

or, taking into account Eqs. (14) and (15):

$$y_j^{\mathrm{ts},1,2} = \pm M_{\mathrm{Tj}} - c_{\mathrm{Tj}}\left(\mu_j N_j - \sqrt{V_{1j}^2 + V_{2j}^2}\right) \leq 0 \tag{24}$$

Considering the approximation assumed for Coulomb criterion through Eq. (11), the yield function expressed by Eq. (24) can be linearized with 8 hyperplanes obtained through the following relationships:

$$y_j^{\mathrm{ts},k} = \pm M_{\mathrm{Tj}} - c_{\mathrm{Tj}}\left(\mu_j N_j - V_{1j}\cos\frac{k\pi}{4} - V_{2j}\sin\frac{k\pi}{4}\right) \leq 0 \tag{25}$$

with $k = 1, 2, \ldots, 8$

The corresponding non-dimensional yield domain is plotted in Fig. 9 and is represented by two octagonal pyramids. It is worth noting that the dimensions of the sides of the non-dimensional octagonal base are not dependant from the contact interface aspect ratio l_1/l_2.

2.3.4.2. Torsion-bending moment interaction The presence of bending moments on interface j moves the center of compression away from the center of the interface, so that a reduced area, herein referred as *effective area*, can be considered for the evaluation of torsion-bending moment interaction. With respect to the effects of shear forces, these are not taken into account in the following formulation and will be specifically addressed in the next section. It is assumed that the normal stresses are uniformly distributed on the effective area and, as a consequence, that the centers of compression and torsion are coincident.

This simplification has been proposed by Casapulla and D'Ayala [18] for a limit analysis problem on arches involving torsion failure and by Orduña and Lourenço [7,12] for 3D limit analysis of rigid blocks assemblages.

The bending moment on interface j is described by its components M_{1j} and M_{2j} which are represented in Fig. 10a with their positive directions, together with the torsion moment M_{Tj}. Adopting the proposed simplification, the eccentricities of the normal force along the reference axes due to bending moments are represented by $e_{1j} = M_{2j}/N_j$ and $e_{2j} = -M_{1j}/N_j$ in Fig. 10b, and the dimensions of the new effective area will be:

$$\begin{aligned} l_{1e} &= l_1 - 2\frac{|M_{2j}|}{N_j} \\ l_{2e} &= l_2 - 2\frac{|M_{1j}|}{N_j} \end{aligned} \tag{26}$$

The only role of the bending moment is to reduce the effective interface area, so that pure torsion failure can be assumed as the failure criterion.

Similar to Eqs. (14) and (17), the yield function associated with this failure criterion is:

$$y_j^{\mathrm{tb},1,2} = \pm M_{\mathrm{Tj}} - M_{\mathrm{T0j,eff}} \leq 0 \tag{27}$$

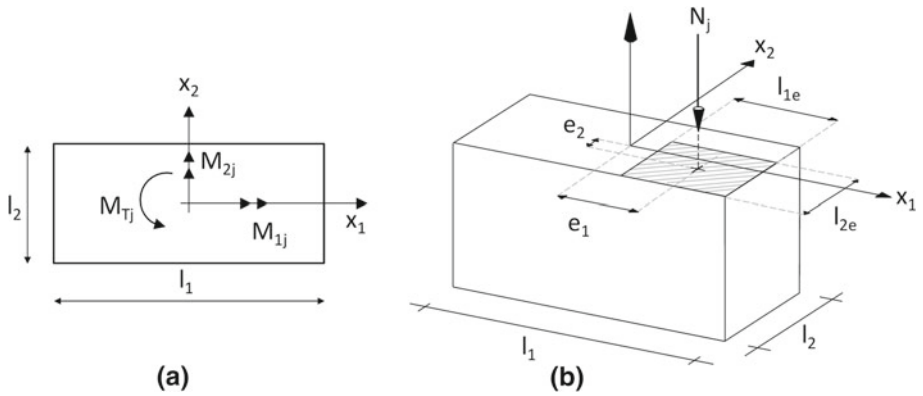

Fig. 10 **a** Torsion-bending moment interaction on the contact interface. **b** Effective area

where

$$M_{\mathrm{T0j,eff}} = c_{\mathrm{Tj,eff}}\,\mu_j N_j \tag{28}$$

and $c_{\mathrm{Tj,eff}}$ is calculated through Eq. (16) by replacing l_1 and l_2 with the effective values l_{1e} and l_{2e}, respectively, given by Eq. (26).

It is worth noting that the torsion strength reduces as the bending moments increase. These were also observed by Orduña and Lourenco [7] that, under the same assumptions, found that if one of the moments takes its maximum value (e.g., M_{2j}), then the torsion strength is not equal to zero but it assumes the value:

$$M_{\mathrm{Tj}} = \frac{1}{4}\mu_j N_j l_2 \tag{29}$$

The yield condition (28), expressed as a function of torsion moment, normal force and bending moments, can still be represented as in Fig. 6, replacing c_{Tj} with $c_{\mathrm{Tj,eff}}$.

2.3.4.3. Effects of bending moment and shear force on torsion strength On the basis of the previous relationships, the combined effects of bending moment and shear force on torsion strength have been taken into account through the following yield functions, expressing the equilibrium condition about the center of effective rectangular area:

$$y_j^{\mathrm{tsb},1,2} = \pm V_{1j}\left|e_{2j}\right| \pm V_{2j}\left|e_{1j}\right| \pm M_{\mathrm{Tj}} - M_{\mathrm{T0j,eff}}\left(1 - \frac{\sqrt{V_{1j}^2 + V_{2j}^2}}{V_{0j}}\right) \le 0 \tag{30}$$

where, as already expressed:

$$e_{1j} = \frac{M_{2j}}{N_j}; \qquad e_{2j} = -\frac{M_{1j}}{N_j}; \qquad M_{\mathrm{T0j,eff}} = c_{\mathrm{Tj,eff}}\,\mu_j N_j \tag{31}$$

Equation (30) can be linearized as follows:

$$y_j^{\mathrm{tsb,k}} = \left(\cos\frac{k\pi}{4} \pm \frac{\left|M_{1j}\right|}{N_j}\cdot\frac{1}{c_{\mathrm{Tj,eff}}}\right)V_{1j} + \left(\sin\frac{k\pi}{4} \pm \frac{\left|M_{2j}\right|}{N_j}\cdot\frac{1}{c_{\mathrm{Tj,eff}}}\right)V_{2j} - \mu_j N_j \pm \frac{1}{c_{Tj,eff}}M_{\mathrm{Tj}} \le 0 \tag{32}$$

with $k = 1, 2, \ldots, 8$

It should be noted that in the case of torsion-shear-bending moment interaction on the contact interface, the center of compression is away from the center of torsion.

The plot of the non-dimensional yield domain is proposed in Fig. 11.

It can be noted that the effect of bending moment is the contraction of the yield domain for torsion and shear interaction in Eq. (25). The modification in the shape of the yield domain depends on the dimensions of the effective area, according to Eq. (32).

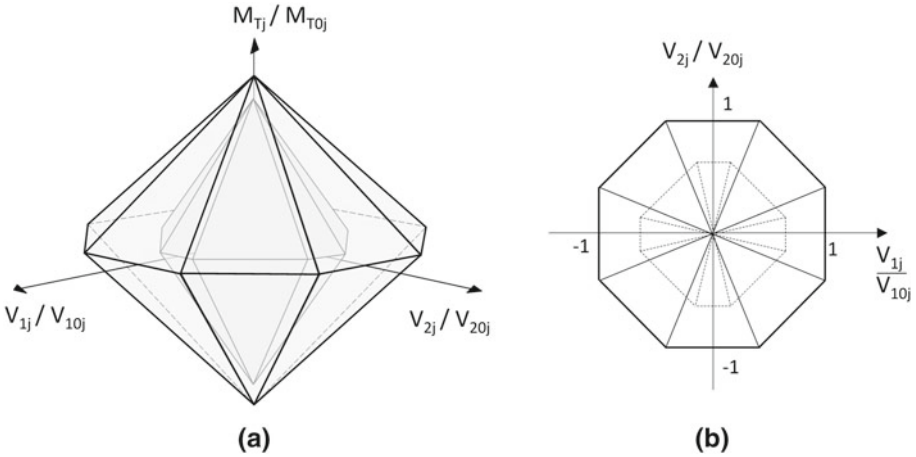

Fig. 11 Yield surfaces for torsion, shear and bending moment interaction

Table 1 Flow directions for rocking

Flow multiplier	γ_{1j}	γ_{2j}	ε_j	θ_{1j}	θ_{2j}	θ_{Tj}
$z_{r1,2}$	0	0	$-l_2/2$	± 1	0	0
$z_{r3,4}$	0	0	$-l_1/2$	0	± 1	0

2.4 Modelling flow rule

Flow rule provides relationships between contact strain rates **q** and the vector of plastic flow multipliers **z** and is governed by the following equations:

$$\mathbf{q} = \mathbf{V}\mathbf{z} \tag{33}$$

where **V** is the flow rule matrix, being $\mathbf{z} \geq \mathbf{0}$ to ensure energy dissipation of the structural system under applied loads.

In this paper, an associative frictional behavior at interfaces is assumed. In case of associative flow rule, the vector of generalized strains is perpendicular to the yield function **y**, and it results [9]:

$$\mathbf{V} = \mathbf{N} \tag{34}$$

being **N** the transpose of the yield function matrix.

As a consequence, the components of resultant strain rate which is perpendicular to the failure surface can be derived from coefficients of yield functions.

The definition of the plastic behavior of joints is completed by the complementarity relation:

$$\mathbf{y}^T\mathbf{z} = 0 \tag{35}$$

which allows to have positive components of flow multipliers **z** only when the stress state is on a yield plane.

The strain rates components related to different collapse modes under the assumption of associative flow rule are illustrated in the following for the sake of clarity.

2.4.1 Rocking

In terms of generalized strains or relative displacement rates related to the interface centroid, the flow consists of relative rotations and relative normal displacements. It is well known that these flow components can be obtained through the associated flow conditions for each component of the bending moment, as shown in Fig. 3. The flow directions for rocking are summarized in Table 1 and sketched in Fig. 12.

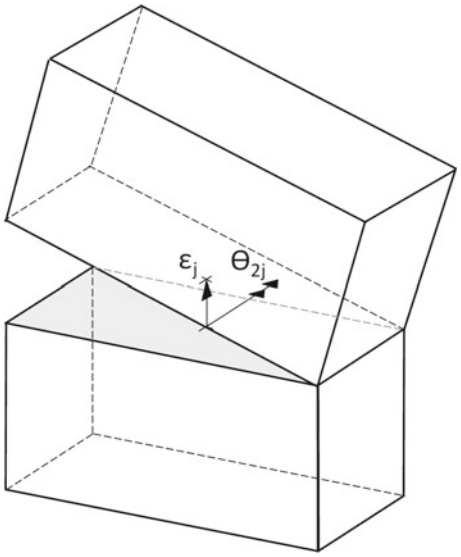

Fig. 12 Associated strain rates for rocking

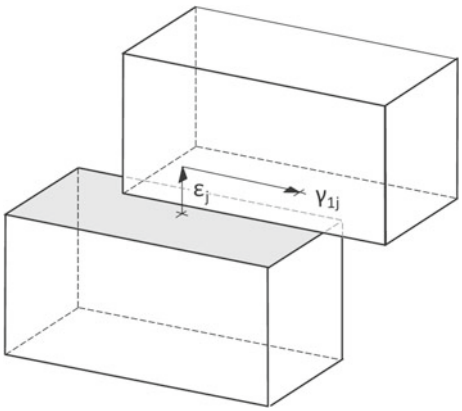

Fig. 13 Associated strain rates for sliding

Table 2 Flow directions for sliding

Flow multiplier	γ_{1j}	γ_{2j}	ε_j	θ_{1j}	θ_{2j}	θ_{Tj}
z_{sk}	$\cos\frac{k\pi}{4}$	$\sin\frac{k\pi}{4}$	$-\mu_j$	0	0	0

2.4.2 Sliding

Considering both components of the shear force, in Fig. 13 the associative flow law is indicated for sliding, and the resultant displacement rates z_{sk} are normal to the corresponding limit surfaces (Fig. 4). Thus, in the associative sliding model adopted in this work, the normality rule is satisfied as dilatancy is considered in the analysis. In Table 2, the flow components for sliding are reported.

2.4.3 Twisting

From a kinematic point of view, in case of associative flow rule, twisting is governed by a displacement rate in the normal direction (dilatancy) and by a relative rotation rate in the same direction, which is characterized by tangential displacement rates always perpendicular to their distance from the center of torsion (Fig. 14).

In particular, the flow components associated with the yield functions given by Eqs. (12) and (17) are reported in Table 3.

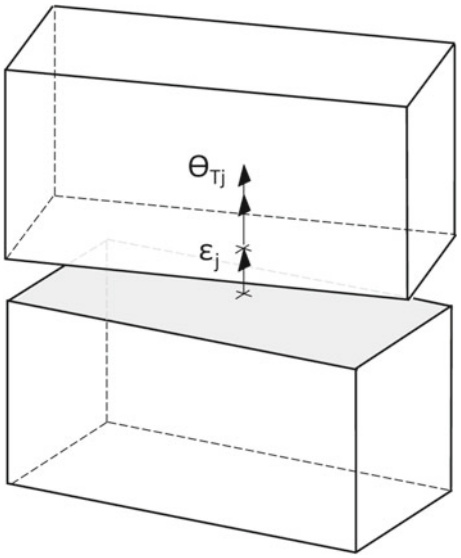

Fig. 14 Associated strain rates for twisting

Table 3 Flow directions for twisting

Flow multiplier	γ_{1j}	γ_{2j}	ε_j	θ_{1j}	θ_{2j}	θ_{Tj}
$z_{t1,2}$	0	0	$-c_{\mathrm{Tj}} \cdot \mu_j$	0	0	± 1

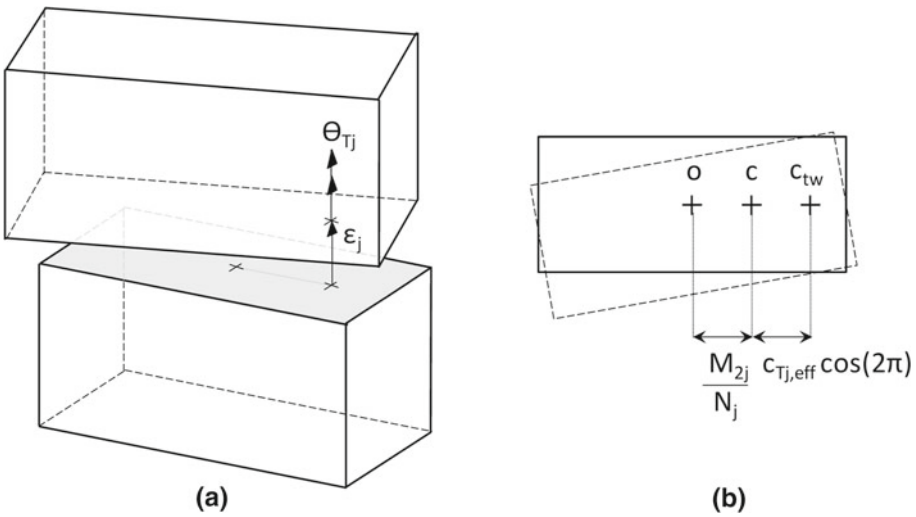

Fig. 15 Associated strain rates for sliding and twisting under bending moment

It is worth noting that in case of non-associated flow law, which is not taken into account in the present study, dilatancy would be zero and normal strain rate $\varepsilon_j = 0$.

2.4.4 Twisting under shear force and bending moment

The flow corresponding to this yield mode consists of a relative rotation in the normal direction about the center of twisting c_{tw} as well as of a displacement rate in the normal direction (Fig. 15). It is worth noting that under the assumption of associative flow rule, this center is different from the center of the effective area.

In particular, with reference to the generalized strains related to the interface center, the flow consists of the relative normal rotation θ_{Tj} and strain rate ε_j and the relative displacements along the tangential directions γ_{1j} and γ_{2j} (Fig. 15). These are reported in Table 4.

Table 4 Flow directions for sliding and twisting under bending moment

Flow multiplier	γ_{1j}	γ_{2j}	ε_j	θ_{1j}	θ_{2j}	θ_{Tj}
$z_{\mathrm{tsb,k}}$	$c_{\mathrm{Tj,eff}} \cdot \cos\frac{k\pi}{4} \pm \frac{\lvert M_{1j}\rvert}{N_j}$	$c_{\mathrm{Tj,eff}} \cdot \sin\frac{k\pi}{4} \pm \frac{\lvert M_{2j}\rvert}{N_j}$	$-c_{\mathrm{Tj,eff}} \cdot \mu_j$	0	0	± 1

2.5 Compatibility conditions

Another constraint to the limit analysis problem is represented by the geometric compatibility condition, relating nodal displacement **u** and contact strain rates **q**, the latter being expressed as a function of matrix **N** and resultant strain rates **z**, according to the assumed flow rule.

This condition is expressed through the following relationship:

$$\mathbf{N}\mathbf{z} = \mathbf{A}^T\mathbf{u} \tag{36}$$

2.6 Energy dissipation

This relation involves positive energy dissipation under live loads. To simplify the formulation of the mathematical program, it is convenient to normalize this requirement assuming [19]:

$$\mathbf{f}_{\mathrm{L}}^T\mathbf{u} = 1 \tag{37}$$

3 Formulation of the limit analysis problem

On the basis of previous governing equations, the limit analysis problem can be formulated in terms of a symmetric mixed complementarity problem with nonlinear constraints (NLMCP) as follows [9]:

$$\begin{bmatrix} \cdot & \cdot & \mathbf{f}_{\mathrm{L}}^T & \cdot \\ \cdot & \cdot & -\mathbf{A}^T & \mathbf{N}(\mathbf{x}) \\ -\mathbf{f}_{\mathrm{L}}^T & \mathbf{A} & \cdot & \cdot \\ \cdot & -\mathbf{N}^T(\mathbf{x}) & \cdot & \cdot \end{bmatrix} \cdot \begin{bmatrix} \alpha \\ \mathbf{x} \\ \mathbf{u} \\ \mathbf{z} \end{bmatrix} + \begin{bmatrix} \cdot \\ \cdot \\ \cdot \\ \mathbf{y} \end{bmatrix} = \begin{bmatrix} 1 \\ \cdot \\ \mathbf{f}_{\mathrm{D}} \\ \cdot \end{bmatrix}$$

$$-\mathbf{y} \geq \mathbf{0} \qquad \mathbf{z} \geq \mathbf{0} \qquad \mathbf{y}^T \cdot \mathbf{z} = 0 \tag{38}$$

where dots correspond to zero-values quantities.

The nonlinearity of the problem is a consequence of the formulation of yield functions taking into account interaction effects ($\mathbf{N} = \mathbf{N}(\mathbf{x})$). Symmetry is related to the assumption on the associativity of flow rule ($\mathbf{V} = \mathbf{N}$).

The NLMCP was solved by means of the iterative procedure described in the following section and based on linear programming.

4 The iterative solution procedure

In order to find a solution to the NLMCP and to overcome the nonlinearity of constraints related to torsion-shear-bending moment interactions, an iterative procedure based on the solution of linear problems has been formulated, as it will be presented in this section.

The MCP has been uncoupled into two LPs corresponding to a lower bound and upper bound formulation.

On the basis of previous relations, the formulation of the lower bound approach for limit analysis is:

$$\begin{aligned} &\max && \alpha \\ &\text{subject to:} && \mathbf{A}\cdot\mathbf{x} = \mathbf{f}_{\mathrm{D}} + \alpha\mathbf{f}_{\mathrm{L}} \\ &&& \mathbf{N}^T(\mathbf{x})\cdot\mathbf{x} \leq \mathbf{0} \end{aligned} \tag{39}$$

where α is the load factor.

The dual mathematical programming problem, whose main variables are the displacement rates, is the formulation of the upper bound formulation and can be expressed as:

$$\begin{array}{ll} \min & -\mathbf{f}_{\mathrm{D}}^{T}\mathbf{u} \\ \text{subject to:} & \mathbf{f}_{\mathrm{L}}^{T}\mathbf{u}=1 \\ & -\mathbf{A}^{T}\mathbf{u}+\mathbf{N}\left(\mathbf{x}\right)\mathbf{z}=\mathbf{0} \\ & \mathbf{z}\geq\mathbf{0} \end{array} \tag{40}$$

The solution procedure is organized as follows.

At first iteration, initial yield functions are used for contact interfaces. For the calculation of initial yield functions, it is assumed $e_{1j}=e_{2j}=0$. In particular, it results:

$$M_{1j,\mathrm{iter}=1}=M_{2j,\mathrm{iter}=1}=0;\ N_{j,\mathrm{iter}=1}=\varepsilon; \tag{41}$$

where ε is a small positive number used to avoid division by zero. This assumption involves that at first step, the effective area is coincident with the whole contact interface.

In the next iterations, the calculation of the dimensions of the effective area l_{1e} and l_{2e} and factor c_{Teff} is carried out on the basis of the results of previous iterations assuming:

$$N_{j,\mathrm{iter}}=\beta\cdot N_{j,\mathrm{iter}-1}+(1-\beta)\cdot N_{j,\mathrm{iter}} \tag{42}$$

where β is an algorithm parameters introduced according to Gilbert et al. [13] to avoid cycling during iterations. Similar relationships are used for bending moments.

Yield functions (27) and (32) are updated on the basis of previous values and programs (39) and (40) are solved to find out static and kinematic unknown variables. The iterative procedure for interaction effects on torsion strength stops when the prescribed convergence tolerance is reached. In particular, the convergence is attained if the following inequality is satisfied:

$$\frac{|\alpha_{\mathrm{iter}}-\alpha_{\mathrm{iter}-1}|}{\alpha_{\mathrm{iter}}}\leq\text{tolerance} \tag{43}$$

being α_{iter} and $\alpha_{\mathrm{iter}-1}$ the collapse load multipliers computed at iteration no. iter and iter-1, respectively.

5 Validation and comparisons

A computer program was generated on the basis of the proposed formulation. For the solution of the linear mathematical problem, the Mosek optimization software was used (www.mosek.com). The program computes as output the failure loads and provides a plot of the corresponding collapse mechanisms.

The program was first verified against the associative solutions obtained on the set of 2D wall panels by Ferris and Tin-Loi [9] and Gilbert et al. [13]. The obtained results were in perfect agreement with the outcomes of two-dimensional modelling formulations.

Afterward, the formulation was compared against the results of experimental investigation on a wall sample constrained at one edge as well as with the outcomes of a similar numerical case study examined by Orduña and Lourenco [7,12].

Finally, two case studies selected from the set of wall panels investigated by Restrepo-Vélez and Magenes [14] were considered for comparison with experimental tests.

In the following, the results of the validation study are presented, comparing numerical and experimental outcomes. As for algorithm parameters, the value of β used in the models was taken as 0.8, and the convergence tolerance was set to 1e-4.

5.1 Masonry walls out-of-plane loaded and constrained at one edge

5.1.1 Experimental case study

In this section, the results of experimental testing and limit analysis of a dry-jointed masonry wall constrained at one edge are presented. Two specimens made of dry-jointed tuff masonry with dimensions of

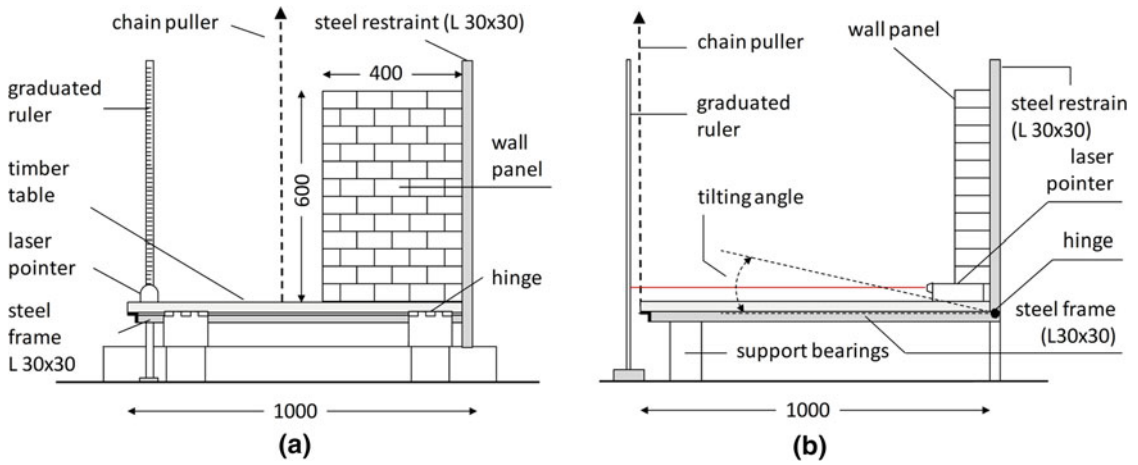

Fig. 16 Test setup

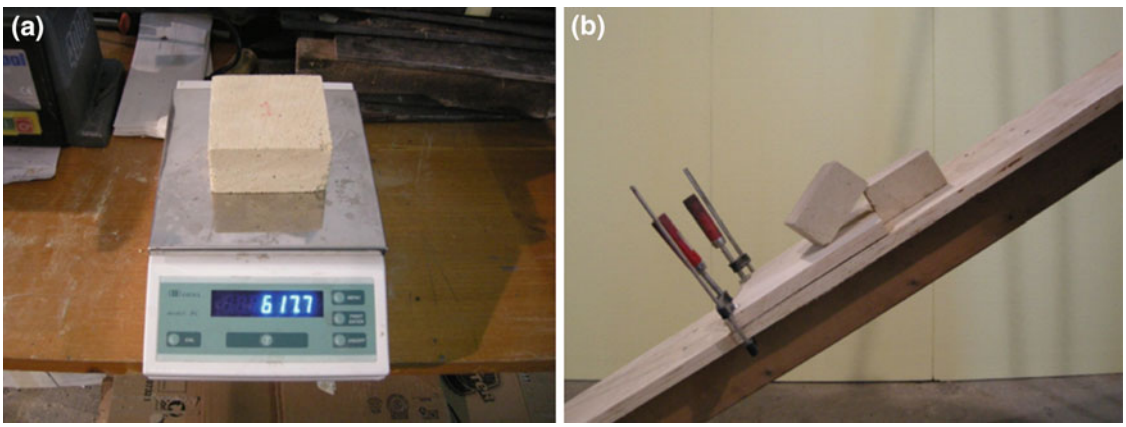

Fig. 17 Measurement of self-weight (**a**) and testing on friction coefficient (**b**)

400 × 100 × 600 mm were prepared for testing, herein named as sample n.1 and n.2. The size of the units is 100 × 100 × 50 mm.

The test setup is simply composed of a timber tilting table 1,000 × 1,000 mm. The table is supported by a steel frame hinged at one edge. A vertical L profile is welded to the supporting frame to provide lateral restraint for the wall (Fig. 16).

The collapse of the masonry panels is induced by progressive tilting of the table, which is lifted up by a chain puller. As a consequence, the blocks are subjected to dead loads equal to self-weight and to horizontal variable loads proportional to the weight and tilting angle. This type of experimental setup has been widely used in the past to investigate the behavior of masonry walls under seismic actions and to take into account the contribution of the distribute masses in the structure [20–22].

The collapse load multiplier was evaluated through the inclination of the table at incipient failure. The angle of the table at collapse was measured with a laser beam pointing at a graduated ruler and verified with an electronic inclinometer.

The tests were monitored by means of two video cameras positioned at opposite points of view. The collapse load multiplier measured from the tilting angle was appreciated with an accuracy of about ±0.005, which is considered acceptable for the research purposes.

The friction angle of the blocks interfaces used for calculations was determined by means of sliding tests and is equal to 0.51. The self-weight is 12.1 kN/m^3 (Fig. 17).

Similar results were obtained for the two specimens. The failure mechanism obtained from tests on wall sample n.1 is shown in Fig. 18. It can be noted the formation of two concentrated diagonal cracks, developing from the base and from the top to the seventh course, respectively, with an inclination angle corresponding

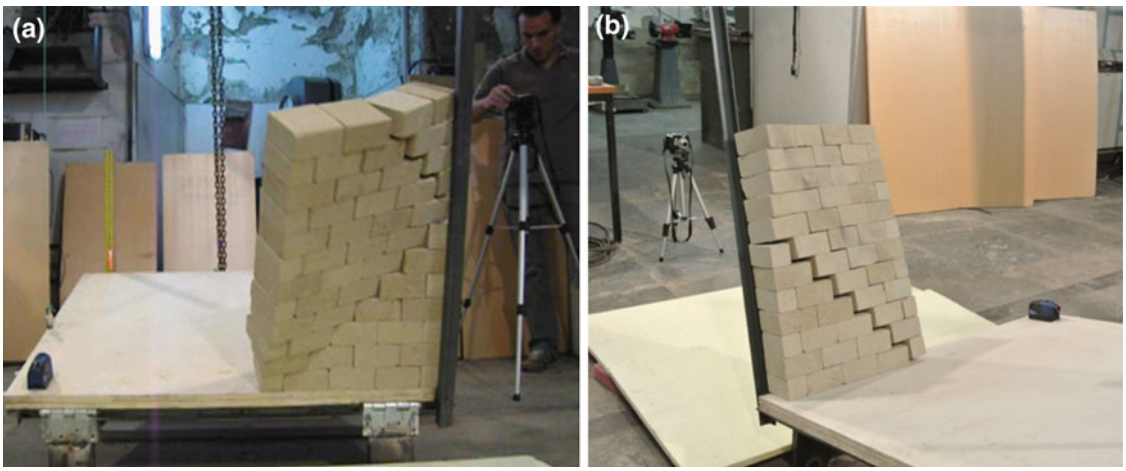

Fig. 18 Experimental failure mode of sample n.1, **(a)** front view and **(b)** back view

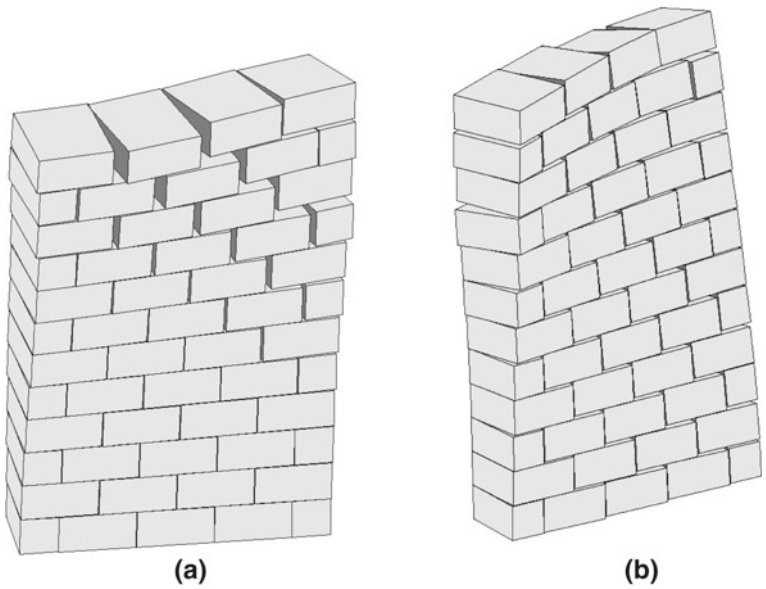

Fig. 19 Plot of the failure mode obtained from the computer program at first step of the analysis, **(a)** front view and **(b)** back view

to the unit staggering aspect ratio. The collapse mechanism of the panel can be schematized with three rigid blocks separated by diagonal yield lines.

The predicted collapse mechanism and load multiplier are shown in Figs. 19 and 20 and Table 5 at first and last iteration. The failure mode computed at the beginning of the procedure, that is for iteration number 1, corresponds to the solution obtained assuming that the effective area is equal to the whole contact interface. The collapse mechanism calculated for the last iteration, that is at convergence, takes into account the effects of reduced area on yield conditions for torsion-shear-bending moment interactions.

The comparison of the failure modes shows that the collapse mechanism predicted for the last step is characterized by discrete diagonal cracks which propagate from the base and the top of the panel. On the contrary, the distribution of strain rates at collapse appears to be smeared for the solution computed at first iteration, that is, neglecting bending moment effects on the dimension of the effective area.

As for the last iteration, a good agreement of experimental and numerical results can be noted. Nevertheless, the failure pattern at the top part of the panel appears to be distributed along three main cracks rather than concentrated along a single crack as observed in experimental tests. In Fig. 21, the computed failure load is plotted against the number of iterations carried out to take into account the nonlinearity due to torsion-shear-bending moment interactions. It can be noted that the number of iterations required for convergence in the

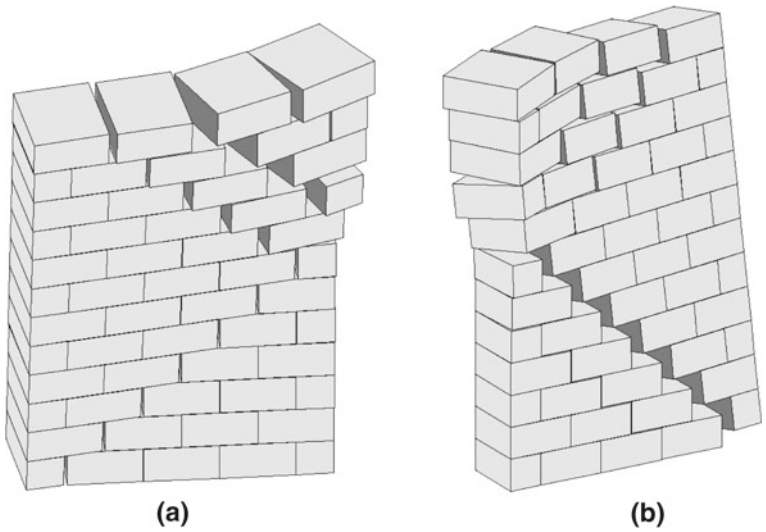

Fig. 20 Plot of the failure mode obtained from the computer program at convergence, **(a)** front view and **(b)** back view

Table 5 Experimental case study constrained at one edge: collapse load multipliers

Specimen	α_{Exp}	Rigid block model size ($b \times c$)	Proposed formulation first iter		Proposed formulation last iter	
			CPU Time (min)	α	CPU Time (min)	α
Sample n. 1	0.275	54 × 138	0.01	0.354	0.05	0.274
Sample n. 2	0.260					

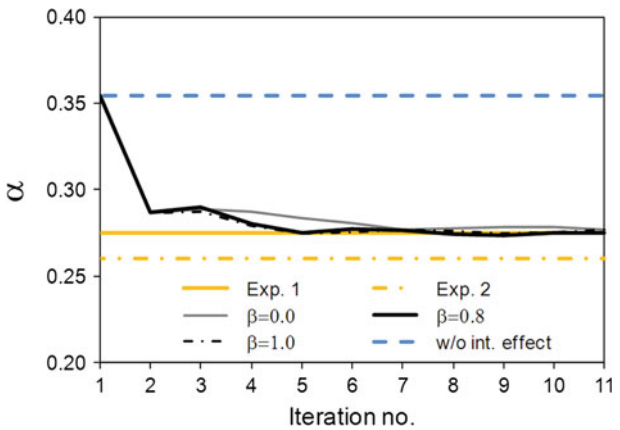

Fig. 21 Computed failure load at different iterations

procedure for the interaction effects is 9. Time required to solve this problem was 0.05 min on a 3.3GHz Intel Xeon Processor E3-1245 with 8.0 GB of RAM.

It is interesting to point out the remarkable difference of the predicted failure load multiplier between the case with no interaction of bending moment on shear and torsion strength and the case with interactions.

To assess the influence of the algorithm parameter β on the convergence behavior, a sensitivity analysis was carried out. In Fig. 21, the curves obtained for $\beta = 0.0$ and $\beta = 1.0$ are plotted for comparison with the default value of 0.8. The analysis shows that the influence of β on the predicted collapse load multiplier is negligible, thus confirming the robustness of the implemented procedure. For β different than the default value, it was noted that the iterative procedure might take more steps to converge. A similar behavior has been observed for the case studies presented in the following.

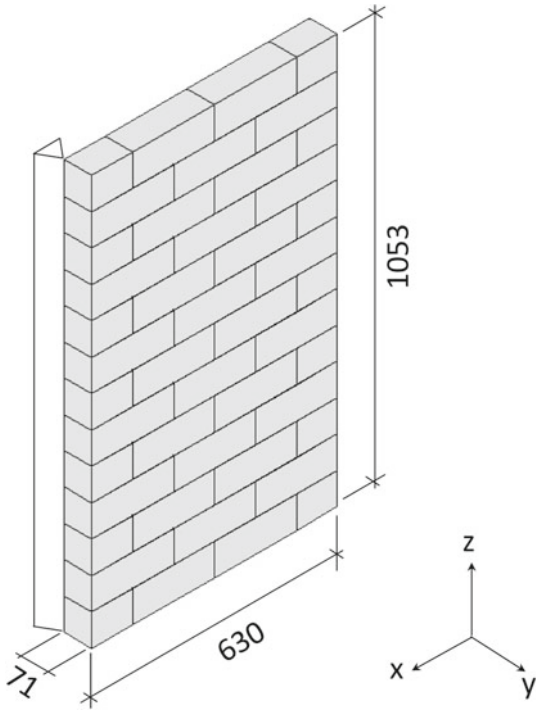

Fig. 22 Rigid block model of the numerical case study

Table 6 Numerical case study constrained at one edge: collapse load multipliers

Case study	Orduña and Lourenço formulation [12] α	Rigid block model size ($b \times c$)	Proposed formulation first iter		Proposed formulation last iter	
			CPU time (min)	α	CPU time (min)	α
Wall constrained at one edge	0.216	46×111	0.01	0.228	0.03	0.182

5.1.2 Numerical case study

The numerical case study investigated in Orduña and Lourenço [12] was analyzed for comparison, even though a different 3D limit analysis formulations have been adopted by the authors.

The panel is made of rigid blocks with dimensions equal to $0.081 \times 0.210 \times 0.07$ m and tensionless contact interfaces. The dimensions of the wall and boundary conditions are shown in Fig. 22.

The wall is supported on the base and is horizontally constrained at one edge. The friction coefficient is 0.7. The self-weight considered for dead loads is 20 kN/m^3. The panel is subjected to out-of-plane horizontal unit forces applied to the centroid of each block.

For the analysis of the wall panel, Orduña and Lourenço [12] adopted a non-associative friction law, and an iterative procedure of MCP was used to solve the limit analysis problem. Moreover, a different linearization of the torsion-shear yield domain was used based on a three linear piecewise discretization.

The computational model of the wall sample consists of 46 blocks and 111 contact interfaces.

The results of the limit analysis are shown in Fig. 23, and the values obtained for collapse load factors are reported in Table 6.

The plot of the failure mode shows the formation of distributed diagonal cracks from the base of the wall panel, (see Fig. 23a). Further diagonal cracks along the opposite direction can be noted from the top of the panel (Fig. 23b).

The comparison with results obtained by Orduña and Lourenço [12] shows a good agreement in terms of predicted collapse load multiplier and failure mode, although in this case yield lines and collapse mechanism are concentrated along two main cracks, similarly to the case study presented in previous section.

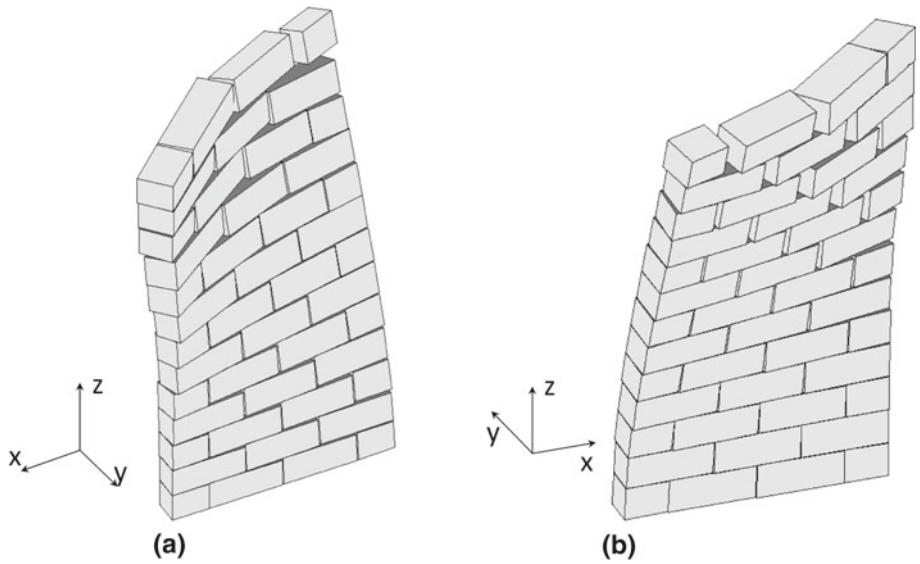

Fig. 23 Plot of the failure mode for the numerical case study

Table 7 Computational results for wall sample S13

Specimen	α_{Exp}	Rigid block model size ($b \times c$)	Proposed formulation first iter		Proposed formulation last iter	
			CPU time (min)	α	CPU time (min)	α
S13	0.181	273 × 756	1.2	0.232	6.5	0.173

Nevertheless, it is clear that although some discrepancies can be found comparing the results provided by the two numerical models, those can be mainly ascribed to the different formulation of the limit analysis problem.

5.2 Masonry panels out-of-plane loaded with perpendicular walls

In this section, further case studies from the literature involving larger number of blocks and different configurations of wall panels were investigated for validation. The efficiency of the proposed simplified formulations in terms of CPU time was evaluated as well.

The considered wall samples are the masonry panels tested by Restrepo-Vélez and Magenes and Restrepo-Vélez et al. [14,15] to analyze out-of-plane mechanisms involving overturning of a front wall and interactions with perpendicular masonry walls.

The specimens were built with dry-jointed marble bricks with nominal dimensions of 80 × 40 × 30 mm. The average value of volumetric weight was 27.3 kN/m^3. The friction coefficient considered for calculation is 0.7, in accordance with experimental values determined for different values of vertical stress.

5.2.1 Front panels with one sidewall

The numerical models generated for the wall samples with one sidewall are depicted in Figs. 24a and 25a. The investigated walls are the specimens S12 and S13 [13,14] which present different lengths of the façade, with the purpose of studying the influence of wall length on the collapse multiplier and the general behavior of the mechanism.

The results of limit analysis are presented in Figs. 24b and 25b and Tables 7 and 8.

The formation of a diagonal crack going from the bottom part of the front walls can be noted, thus involving the activation of a rigid block mechanism in the panel. For wall panel S12, the formation of a yield line from the top course is predicted as well, similar to the experimental case study presented in previous section. Interaction effects with perpendicular walls are also evident, producing in-plane and inward displacements at the top of the

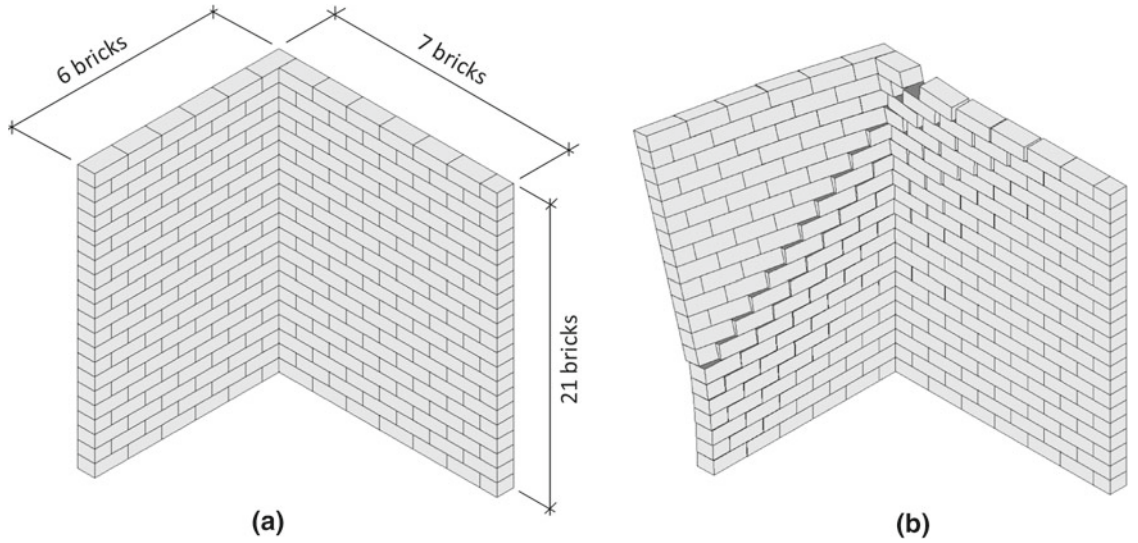

Fig. 24 S13 wall panel. **(a)** Configuration of the specimen and **(b)** plot of the failure mode

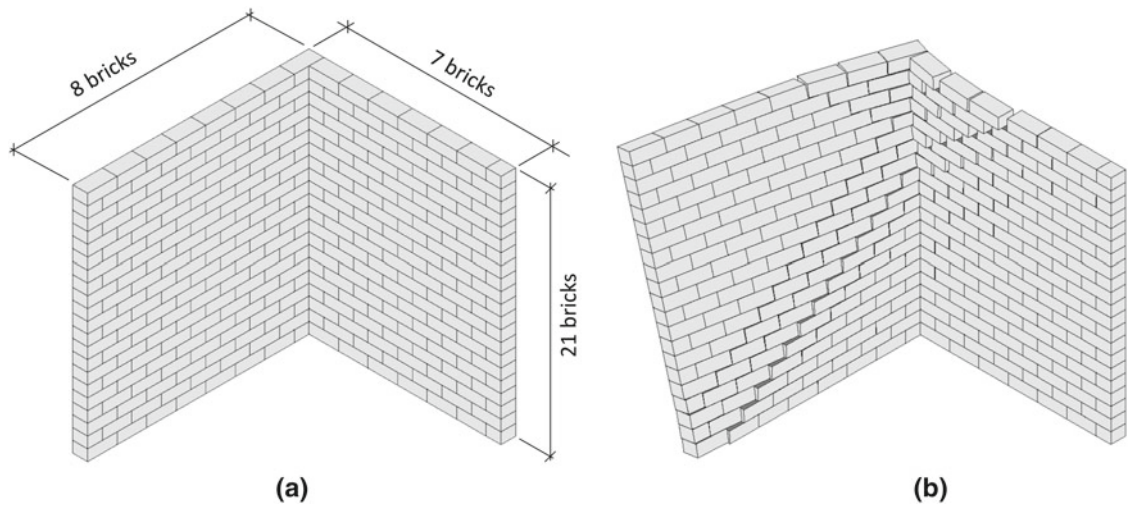

Fig. 25 S12 wall panel. **(a)** Configuration of the specimen and **(b)** plot of the failure mode

Table 8 Computational results for wall sample S12

Specimen	α_{Exp}	Rigid block model size ($b \times c$)	Proposed formulation first iter		Proposed formulation last iter	
			CPU time (min)	α	CPU time (min)	α
S12	0.129	315 × 882	5.3	0.186	33.7	0.137

panel next to the connection with the front wall. CPU time required for calculations is reasonable, considering the dimension of the limit analysis problems.

The predicted failure mechanism and collapse load multiplier are in accordance with experimental evidence although some difference occurs. In particular, for test S13, the formation of a clear diagonal crack going from the top course to the connection with the perpendicular wall can be noted as well. On the contrary, in the numerical model, a smeared crack pattern is predicted for this wall sample.

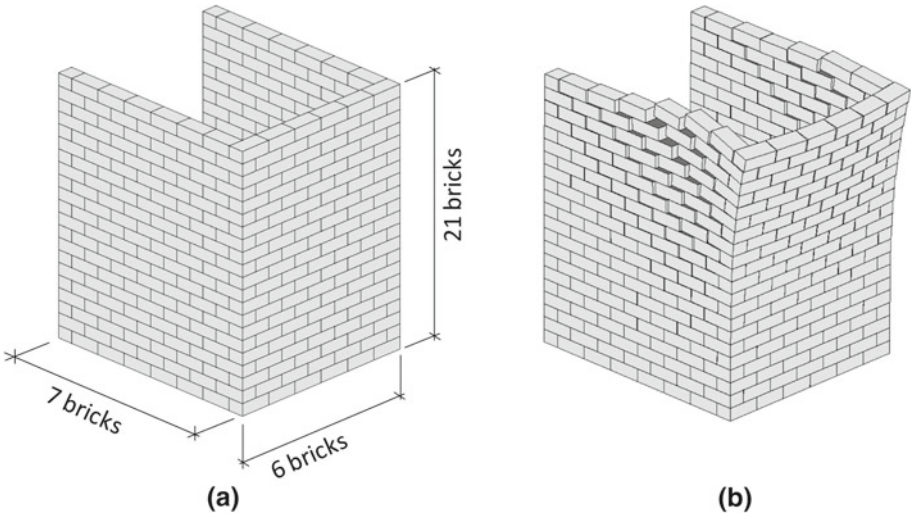

Fig. 26 S9 wall panel. **(a)** Configuration of the specimen and **(b)** plot of the failure mode

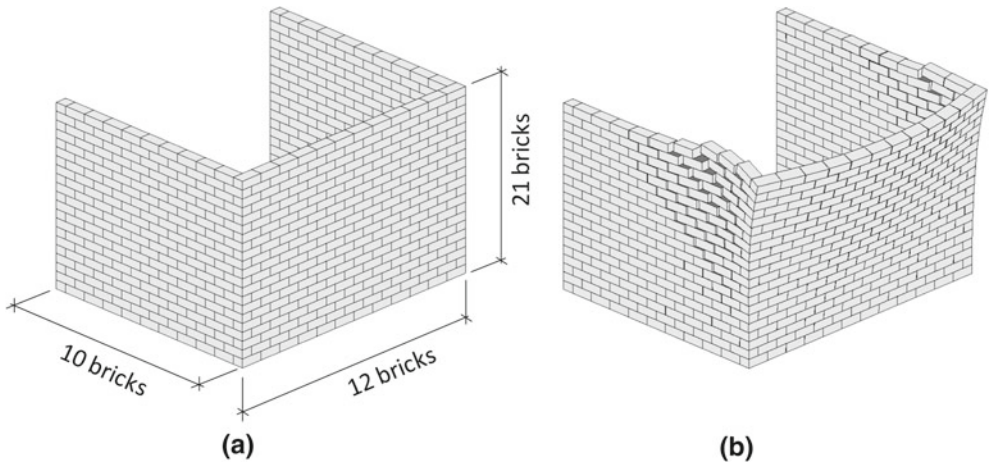

Fig. 27 S10 wall panel. **(a)** Configuration of the specimen and **(b)** plot of the failure mode

Table 9 Computational results for wall sample S9

Specimen	α_{Exp}	Rigid block model size ($b \times c$)	Proposed formulation first iter		Proposed formulation last iter	
			CPU time (min)	α	CPU time (min)	α
S9	0.352	410 × 1,145	3.7	0.387	15.1	0.362

5.2.2 Front panels with two side walls

Masonry wall assemblages investigated in this section are the samples S9 and S10 tested in Restrepo-Vélez et al. [15].

The configuration of the examined wall samples and overall dimensions are shown in Figs. 26a and 27a.

The results of the analysis are reported in Tables 9 and 10 and Figs. 26b and 27b.

The numerical failure modes involve the in-plane collapse of the side walls and the overturning of the top part of the front panel. From the plot of deformed shape at failure, it can be noted that the out-of-plane displacements of the façade are distributed throughout the panel. CPU time required for calculations was 15.1 and 60.8 min for S9 and S10 wall panels, respectively.

Also in this case, the predicted failure mechanisms and collapse load multiplier are in a good agreement with experimental tests.

Table 10 Computational results for wall sample S10

Specimen	α_{Exp}	Rigid block model size ($b \times c$)	Proposed formulation first iter		Proposed formulation last iter	
			CPU time (min)	α	CPU time (min)	α
S10	0.213	662 × 1,901	23.0	0.262	60.8	0.215

The failure mode observed from experimental tests is the overturning of façades along an horizontal hinge and involves the upper courses of stones in both cases. In-plane rocking and sliding failure mechanisms of perpendicular walls were observed as well, according to the numerical model.

6 Conclusions

In this paper, a three-dimensional limit analysis formulation based on linear programming was presented. The formulation is based on convex contact interface models and associative flow rule for strain rates. Simplified yield conditions have been used to take into account torsion and shear failures. A linearized yield function has been proposed to take into account interaction effects of torsion strength with shear stresses and bending moments.

The limit analysis problem has been formulated in terms of nonlinear mathematical programming and solved by means of an iterative solution procedure based on linear sub-problems.

Validations and comparisons were carried out against numerical case studies and experimental tests.

The results showed that the proposed formulation, although simplified and based on associative flow rule, provides a good prediction of experimental results in reasonably short computational time. In particular, the results obtained from limit analysis show the effects of reduced contact area and shear forces on torsion strength according to the proposed formulation of the yield functions, and it is also shown how the effects of torsion-shear-bending moment interactions involve a remarkable reduction of collapse load factor.

Nevertheless, it should be pointed out that in some cases, differences with experimental failure modes were observed. Of course, these differences could be ascribed to factors affecting experimental results, such as stress concentrations due to dry joints or geometric imperfections in the specimens, as well as to the simplified assumption made for the formulation of the limit analysis problem.

For these reasons, further developments of the present study include iterative solution procedures based on linear programs for non-associative friction rules with zero dilatancy, piecewise multi-linear approximation of torsion-shear yield function and the use of limited compressive strength to take into account crushing as well. Finally, it would be interesting to use parallel computing, which has not been implemented in this work, to take advantage of multiple processors to further speed up solution times.

Acknowledgments A part of the present study was carried out in the framework of the three-year RELUIS2 Project-Line 1-Task 1 (2010–2013). The authors wish to express their gratitude to Mario Torricella from the Laboratory of Architecture in Naples, for his assistance and support in the preparation of the specimens, test setup and throughout the execution of experimental investigations.

References

1. Livesley, R.K.: Limit analysis of structures formed from rigid blocks. Int. J. Numer. Methods Eng. **12**, 1853–1871 (1978)
2. Gilbert, M., Melbourne, C.: Rigid-block analysis of masonry structures. Struct. Eng. **72**(21), 356–361 (1994)
3. Orduña, A., Lourenço, P.B.: Limit analysis as a tool for the simplified assessment of ancient masonry structures. In: Lourenço, P.B., Roca, P. (eds.) Proceedings of 3rd International Seminar on Historical Constructions, pp. 511–520. University of Minho Press, Guimarães (2001)
4. Roca, P., Cervera, M., Gariup, G., Pelà, L.: Structural analysis of masonry historical constructions. Classical and advanced approaches. Arch. Comput. Methods Eng. **17**, 299–325 (2010)
5. Livesley, R.K.: A computational model for the limit analysis of three-dimensional masonry structures. Meccanica **27**(3), 161–172 (1992)
6. Tri, T.-C.: Collapse analysis of block structures in frictional contact. PhD Thesis. School of Civil and Environmental Engineering. The University of New South Wales, Sydney, Australia (2009)
7. Orduña, A., Lourenço, P.B.: Three-dimensional limit analysis of rigid blocks assemblages. Part I: torsion failure on frictional joints and limit analysis formulation. Int. J. Solids Struct. **42**(18-19), 5140–5160 (2005)
8. Drucker, D.C.: Coulomb friction, plasticity and limit loads. J. Appl. Mech. ASME **21**(1), 71–74 (1954)

9. Ferris, M., Tin-Loi, F.: Limit analysis of frictional block assemblies as a mathematical program with complementarity constraints. Int. J. Mech. Sci. **43**, 209–224 (2001)
10. Baggio, C., Trovalusci, P.: Limit analysis for no-tension and frictional three-dimensional discrete systems. Mech. Struct. Mach. **26**, 287–304 (1998)
11. Baggio, C., Trovalusci, P.: Collapse behaviour of three-dimensional brick block systems using non-linear programming. Struct. Eng. Mech. **10**(2), 181–195 (2000)
12. Orduña, A., Lourenço, P.B.: Three-dimensional limit analysis of rigid blocks assemblages. Part II: load-path following solution procedure and validation. Int. J. Solids Struct. **42**(18-19), 5161–5180 (2005)
13. Gilbert, M., Casapulla, C., Ahmed, H.M.: Limit analysis of masonry block structures with non-associative frictional joints using linear programming. Comput. Struct. **84**, 873–887 (2006)
14. Restrepo-Vélez, L.F., Magenes, G.: Static Tests on Dry Stone Masonry and Evaluation of Static Collapse Multipliers. In Research Report ROSE 2009/02, 72. Pavia: IUSS Press (2009)
15. Restrepo-Vélez, L.F., Magenes, G., Griffith, M.C.: Dry Stone Masonry Walls in Bending—Part I: Static Tests. Int. J. Arch. Herit. (2012). doi:10.1080/15583058.2012.663059
16. Casapulla, C., Portioli, f., Maione, A., Landolfo, R.: A macro-block model for in-plane loaded masonry walls with non-associative Coulomb friction. Meccanica (2013). doi:10.1007/s11012-013-9728-5
17. Casapulla, C.: Frictional strength of out-of-plane loaded masonry walls. In: Proceedings of IX National Congress of Earthquake Engineering in Italy (ANIDIS 1999). Turin, 20–23 Sept. 1999 (in Italian) (1999)
18. Casapulla, C., D'Ayala, D.: Lower-bound approach to the limit analysis of 3D vaulted block masonry structures. In: Hughes, T.G., Pande, G.N. (eds.) Computer Methods in Structural Masonry, vol. 5, pp. 28–36. Computers & Geotechnics Limited, Swansea (2001)
19. Maier, G., Nappi, A.: A theory of no-tension discretized structural systems. Eng. Struct. **12**, 227–234 (1990)
20. Ceradini, V.: Modellazione e sperimentazione per lo studio della struttura muraria storica. PhD Thesis, University of Rome 'La Sapienza' (in italian) (1992)
21. Giuffrè, A.: Sicurezza e Conservazione del Centri Storici, Il Caso Ortigia. Bari: Laterza (in Italian) (1993)
22. Nisticò, N., Pagnoni, T.: Osservazioni Sperimentali sul Comportamento Sismico di Strutture a Blocchi e in Muratura, Dept. of Structural Engineering and Geotechnics. University of Rome 'La Sapienza' (in Italian) (1995)